Broadband implementation of coprime linear microphone arrays for direction of arrival estimation[a)]

Dane Bush[b)] and Ning Xiang
Graduate Program in Architectural Acoustics, School of Architecture, Rensselaer Polytechnic Institute, 110 8th Street, Troy, New York 12180, USA

(Received 24 February 2015; revised 12 June 2015; accepted 16 June 2015; published online 21 July 2015)

Coprime arrays represent a form of sparse sensing which can achieve narrow beams using relatively few elements, exceeding the spatial Nyquist sampling limit. The purpose of this paper is to expand on and experimentally validate coprime array theory in an acoustic implementation. Two nested sparse uniform linear subarrays with coprime number of elements (M and N) each produce grating lobes that overlap with one another completely in just one direction. When the subarray outputs are combined it is possible to retain the shared beam while mostly canceling the other superfluous grating lobes. In this way a small number of microphones ($N + M - 1$) creates a narrow beam at higher frequencies, comparable to a densely populated uniform linear array of MN microphones. In this work beampatterns are simulated for a range of single frequencies, as well as bands of frequencies. Narrowband experimental beampatterns are shown to correspond with simulated results even at frequencies other than the arrays design frequency. Narrowband side lobe locations are shown to correspond to the theoretical values. Side lobes in the directional pattern are mitigated by increasing bandwidth of analyzed signals. Direction of arrival estimation is also implemented for two simultaneous noise sources in a free field condition. © *2015 Acoustical Society of America*.
[http://dx.doi.org/10.1121/1.4923159]

[MRB] Pages: 447–456

I. INTRODUCTION

The purpose of this paper is to experimentally demonstrate the frequency-dependent beamforming capabilities of acoustic coprime arrays, which have predictable, highly-directive beampatterns, using relatively few microphones. Microphone arrays are powerful tools which can be used for spatial recording, isolating a signal from noise and reverberation, and locating sound sources.[1–3] Accuracy of source localization and array gain are improved with increasing number of array elements. Using acoustic vector sensors which combine sound pressure and particle velocity shows promise;[4–6] however, these sensors can be expensive. New techniques for improving array performance with fewer conventional microphone elements are the subject of much contemporary research. There has been active research in the area of array implementation during the recent two decades which has seen progress regarding array configurations as well as processing algorithms.[1,2,7–10]

Random sampling is a type of sparse sensing that has been applied to array design, wherein irregular element distribution is used. However construction is non-trivial, as optimization is often computationally demanding, thus sub-optimal solutions may be found using a number of heuristic algorithms such as the Monte Carlo, simulated annealing, golden section search, and conjugate gradient algorithms, or combinations thereof.[11] One approach proposed by Yu and Donohue[12] uses a genetic algorithm for near-field applications, whose search path is guided by objective functions based on microphone placement that have been correlated with increased performance. While not fully random, this approach still requires a computational search and results may be specific to the given acoustic scene. In contrast, coprime sampling follows a deterministic design process and provides an easily predictable output.

These irregular arrays also may be out-performed by uniform arrays at lower frequencies, when aliasing is not a factor, due to elevated side lobe levels.[11] This is addressed by Rigelsford and Tennant[13] for random spherical arrays by broadening the observed bandwidth. Due to the aperiodicity of the side lobe locations, the only common maxima in the patterns collected at multiple discrete frequencies occur at the main beam direction.

Compressive sensing is a method for solving underdetermined problems in signal processing with accurate reconstruction, as long as two conditions are met: that the underlying signal is sufficiently sparse, and that the process mapping the underlying signal to observations is sufficiently incoherent.[8] Its advantages in improving signal to interference ratio over conventional processing are demonstrated in Ref. 9 using simulated and experimental hydrophone data.

Recent developments in uniform linear array processing may still be leveraged by coprime array processing, due to the uniform nature of the coprime subarrays. These include investigations by Bouchard *et al.*[1] which use a weighted combination of sub-beamformers, each using different spatial modes for the source model.

[a)]Aspects of this work have been presented at the 168th ASA Meeting in Indianapolis, Indiana, 2014
[b)]Electronic mail: bushd2@rpi.edu

Crocco and Trucco[7] propose a method of optimizing the mean adherence between the desired and actual directivity pattern (also known as beampattern or directional characteristic), that takes advantage of the relationship between the sampling interval and the element separation of a uniform linear array. Their method reduces the number of operations needed to evaluate the cost function of the filter-and-sum beamformer from $O(N^4L^4)$ to $O(N^3L^2)$, where N is the number of array elements and L is the order of the finite impulse response filter.

Bai *et al.*[2] implemented single input, multiple output (SIMO) processing with three different algorithms for equivalent source inverse filtering (ESIF), in order to increase a signal strength in the presence of noise and reverberation, while simultaneously limiting source distortion. Array signal-to-noise ratio (SNR) gain and speech distortion were evaluated both objectively and subjectively. Though there is a tradeoff between SNR gain and speech distortion, they found that the best compromise was achieved using the SIMO-ESIF combination along with a generalized sidelobe canceller, implemented via blocking matrix.

These represent a broad but shallow cross-section of the current work on arrays. For the most recent comprehensive overview on acoustic array signal processing, see Ref. 11. No coprime arrays have yet been included in the overview though.

Coprime sampling, as proposed by Vaidyanathan and Pal,[14] uses uniform linear subarrays with inter-element spacings which are sparse (exceeding the spatial Nyquist limit), consisting of M and N elements, where M and N are coprime with one another. This sparse sampling produces predictable aliasing, which mostly canceled-out by combining the coprime subarray outputs, as elaborated later. They show that at the given design frequency, the coprime array can theoretically achieve $M \times N$ discrete passbands using two subarray filter banks of just $M + N - 1$ total sample points, given the same aperture length. Simulations are presented with juxtaposed beampatterns of variously-shifted coprime responses, both unweighted and weighted using Remez coefficients.

Weng and Djuri[10] propose a processing algorithm for coprime radar arrays following Vaidyanathan and Pal's work which uses a uniform linear array direction of arrival estimation algorithm (MODE in this case) to locate the source within the unaliased (wrapped) angular range of each subarray; then the Chinese remainder theorem is leveraged so the subarrays can be cross-referenced via discrete phase shifts such that the direction of arrival can be accurately placed within the full (unwrapped) angular domain of the coprime array. Mean square error results are shown, as calculated from numerical simulations.

The aforementioned papers represent a theoretical perspective on coprime arrays. Not much experimental data is yet available on the topic, especially for acoustic application. Xiang *et al.*[15] presented preliminary results of an experimental implementation of a coprime microphone array at the specific design frequency.

This work experimentally validates coprime theory for acoustic application using linear arrays of electret microphones, expanding on Ref. 15 by including a wide range of frequencies in the theoretical discussion as well as the experimental results. The discussion on coprime theory relies heavily on the work of Vaidyanathan and Pal.[14] Conventional fixed spatial beamforming as well as delay-and-sum beamforming are used to obtain the directional characteristic of unweighted coprime arrays at the implied design frequency. In this work "beampattern" refers to directional characteristic measured via one measurement per angle using fixed spatial beamforming, and "directional response" refers to directional characteristic derived using delay-and-sum beamforming on a single measurement. The same processing methods are used to investigate beampatterns of coprime arrays at frequencies below the design frequency. The main advantage of coprime arrays is their ability to observe higher frequencies than those of uniform linear arrays composed of a similar number of elements; however, this work demonstrates that they are still usable at all frequencies in between. Bandpass beampatterns are also explored and are shown to be potentially useful in mitigating aliasing noise in the multiple source case. There is also an issue of array gain, but the focus of this work is to validate the beampattern and beam width against coprime theory.

II. THEORY

For simplicity and fundamental comparison of coprime arrays with uniform linear arrays, conventional beamforming is used and all sources are assumed to be in the array's far-field (i.e., plane waves). Indexing the array elements starting at $m = 0$, the beampattern for an M-element uniform linear array is described by

$$H(e^{j\alpha}) = \sum_{m=0}^{M-1} h(m) e^{-j\alpha m}, \tag{1}$$

where $h(m)$ is the output of the mth element, $j = \sqrt{-1}$, and $\alpha = (2\pi/\lambda) d \sin\theta$, d being the distance between each element, λ the wavelength, and θ the azimuthal angle counterclockwise from normal.[16] $h(m)$ is independent of θ and λ as long as the elements are omni-directional with flat frequency response. Given uniform elements and spacing, and sources in the far-field, the individual element outputs have the same amplitude, $h(m) = h_0$.

The sum can be solved for any value of M and α as follows:[16]

$$H(e^{j\alpha}) = Mh_0 \sum_{m=0}^{M-1} e^{-j\alpha m} = Mh_0 \frac{\sin\left(M\frac{\alpha}{2}\right)}{\sin\left(\frac{\alpha}{2}\right)} e^{-j(M-1)(\alpha/2)}. \tag{2}$$

For decreasing values of d the beampattern converges to a sinc function.

A. Beam width

One of the main qualifiers of microphone arrays is beam width. In most cases, the beam is desired to be as narrow as

possible for the given constraints, without introducing spatial aliasing. Beam width is generally defined as the angle between the zeros on either side of the center beam, shown in Fig. 1(a).[17] By setting the numerator of Eq. (2) equal to zero, the argument of the sine in the numerator must be equal to $\pm\pi$. This means that

$$\sin\theta_{\text{zeros}} = \pm\frac{\lambda}{Md}, \tag{3}$$

thus the beam width is $\theta_{\text{beam}} = 2\arcsin(\lambda/Md)$. Since $d = L/M$, where L is the aperture length, the beam width reduces to

$$\theta_{\text{beam}} = 2\arcsin\left(\frac{\lambda}{L}\right), \tag{4}$$

purely a function of the aperture length relative to the wavelength observed.

For a traditional uniform linear array at its design frequency, element separation is a half-wavelength ($d = \lambda/2$), so Eq. (3) would be simplified to $\sin\theta = \pm 2/M$, which means $\theta_{\text{beam}} = 2\arcsin(2/M)$; for θ close to 0 (normal incidence) this reduces to $\theta_{\text{beam}} = 4/M$.

B. Aliasing

Standard uniform linear array element separation is determined by the observed wavelength and limited by the spatial Nyquist theorem such that the optimal inter-microphone distance is $d_{\text{ULA}} = \lambda/2$. If this element separation is exceeded then aliasing occurs in the angular domain, causing additional beams, called grating lobes,[17] which are identical to and indistinguishable from the main beam.

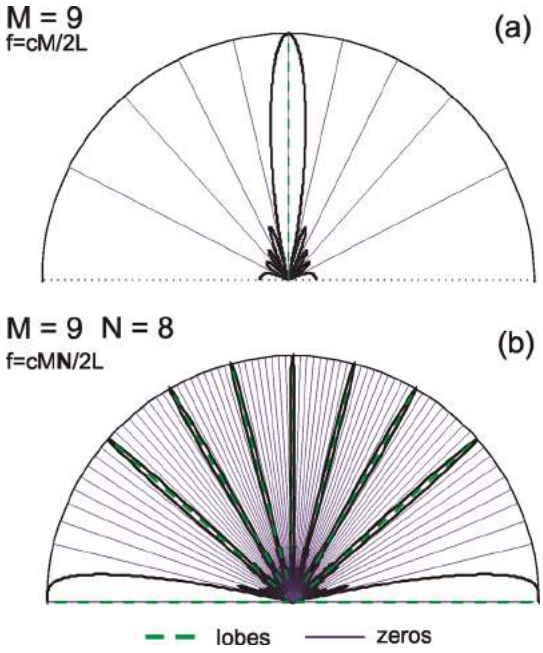

FIG. 1. (Color online) Element separation dependence of M-element array grating lobe and zero locations ($M = 9$). (a) Element separation of $d = \lambda/2$, where λ is the wavelength. (b) Element separation of $d = N\lambda/2$ (in this case $N = 9$).

Coprime array subarrays use sparse uniform spacing,

$$d_{\text{sparse}} = N\frac{\lambda}{2}, \tag{5}$$

where N is an integer. This results in N lobes (including the main beam and grating lobes) between $-90°$ and $90°$.[17]

Although increasing the total number of array elements does help to narrow each beam [per Eq. (3)], only element separation determines aliasing pattern (i.e., number of grating lobes).

Aliasing occurs in the transfer function described by Eq. (1) at phase angles $|\alpha| \geq \pi$, and grating lobes are formed when $\alpha = 2\pi i$, for integers $-N/2 \leq i \leq N/2$.

Since $\alpha = (2\pi/\lambda)d\sin\theta$, grating lobes can be found at physical angles

$$\sin\theta_i = \frac{\lambda}{d}i, \quad -N/2 \leq i \leq N/2, \tag{6}$$

as shown in Fig. 1(b), where $N = 2d/\lambda$ via Eq. (5). This relation holds for any element separation at any frequency. This reduces to just one lobe when using uniform linear array separation, $d_{\text{ULA}} = \lambda/2$, since N would be equal to 1, and the only integer within $\pm N/2$ is 0, therefore the only lobe is the main beam at $\theta_0 = 0$.

Grating lobe width follows Eq. (3) for beam width, so in the case of sparse separation, $\sin\theta_{\text{zeros}}$ is reduced by a factor of $1/N$ for $d_{\text{sparse}} = Nd_{\text{ULA}}$.

C. Coprime arrays

For two integer numbers to be coprime (also known as mutually prime), their largest common divisor must be 1. A coprime receiving array is composed of two parallel, co-located uniform linear subarrays. In this work the subarrays are referred to as M- and N-array, referring not to the spacing factor, but rather the number of elements in the subarray ($M > N$ here by convention). These subarrays have sparse coprime element spacings $d_M = N\lambda/2$ and $d_N = M\lambda/2$, respectively. As long as the aperture of each subarray is the same fixed length, L, the M-array has inter-element separation $d_M = L/M$ and the N-array has inter-element separation $d_N = L/N$. The aliasing significantly narrows the center beam and introduces a coprime number of grating lobes in each subarray. The outputs of each sparse, uniform subarray are multiplied together, which causes their differing grating lobes to mostly cancel one another except in the one shared direction, where they form the main beam of the overall coprime array. Figure 2 shows the beampatterns of aliased subarrays of $M = 5$ and $N = 4$ in broken lines atop a representation of their sparse microphone element distributions. The solid line indicates their combined coprime beampattern.

Since the array length and number of elements in each subarray are fixed, the coprime array has a design frequency, implied by the following relationship:

$$\frac{L}{M} = d_M = N\frac{\lambda}{2}. \tag{7}$$

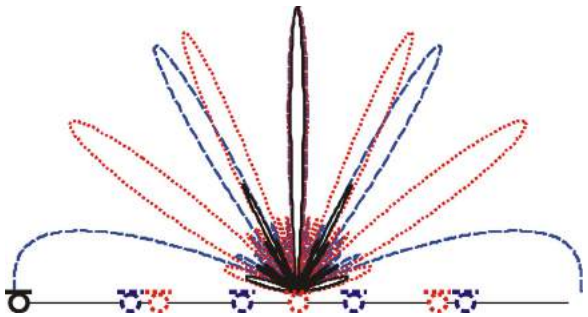

FIG. 2. (Color online) Element distributions and beampatterns of $M = 5$ subarray (dashed lines) and $N = 4$ subarray (dotted lines). The subarray outputs combine to form the coprime array beampattern (solid lines). The solid line microphone element represents a shared element among both subarrays.

Replacing λ by c/f in Eq. (7) leads to the coprime array design frequency

$$f_c = \frac{cMN}{2L}. \tag{8}$$

Through the use of beampattern simulations, Fig. 3 illustrates that the subarray grating lobes still cancel in much the same way at frequencies lower than f_c, providing a singular narrow beam. Although beampatterns are shown for only a few frequencies below f_c, grating lobe cancellation occurs in much the same way for the full range of frequencies. Beam width depends on frequency and aperture length as shown below.

It is important to note that although the upper limit frequency is determined by the coprime number of subarray elements, the beam width is the same as that of a uniform linear array for each respective frequency and is dependent on aperture length [shown by Eq. (4)]. Coprime configuration and processing allows for fewer array elements at the higher frequency, or put another way, it allows for a higher range of frequencies using the same overall number of elements.

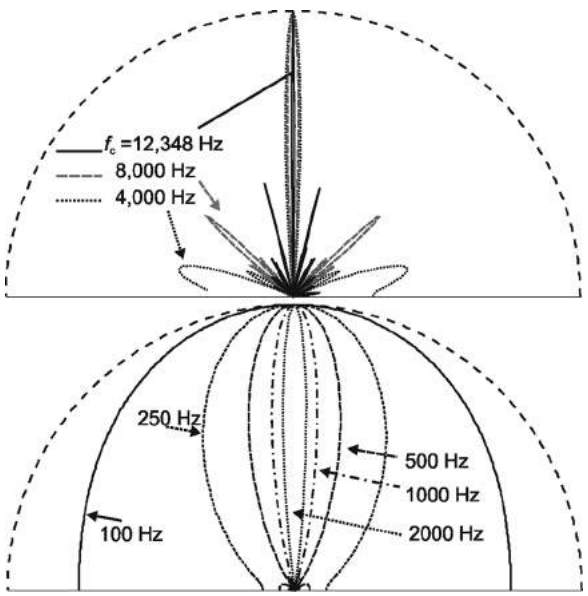

FIG. 3. Computer-modeled coprime array beampatterns for a coprime array with $M = 9$ and $N = 8$ at a few select frequencies taken from the wide range of available operating frequencies below the coprime design frequency, f_c Hz = 12 348 Hz. The maximum side lobe level is 4.1 dB below the main beam for this unweighted coprime array.

D. Coprime beam position and width

The number of grating lobes in the subarray pattern is dependent on frequency and element separation. Using Eq. (5) with $d = L/M$ and solving for number of lobes, n, as a function of frequency, f, leads to

$$n(f) = \frac{2Lf}{cM} \tag{9}$$

for the M-array.

For $f = f_{\text{ULA}} = cM/2L$ (equivalent to $d = \lambda/2$) this reduces to $n = 1$, and for $f = f_c = cMN/2L$, this reduces to $n = N$. In other words,

$$1 \le n \le N \quad \text{for} \quad f_{\text{ULA}} \le f \le f_c, \tag{10}$$

where n is the number of lobes.

Again with $d = L/M$ and substituting frequency-dependent n for N, the equation for grating lobe location [see Eq. (6)] becomes

$$\sin\theta_i = \frac{M\lambda}{L} i, \quad -n/2 \le i \le n/2, \tag{11}$$

where $n = 2Lf/cM$. The other subarray has the same length and is operated at the same frequency, but has N elements. Therefore, the N-array has $m = 2Lf/cN$ grating lobes at positions $\sin\theta_j = (M\lambda/L)j$, where $-m/2 \le j \le m/2$.

Knowing the frequency-dependent positions of each subarray's grating lobes allows one to prove that grating lobe cancellation occurs similarly for any frequency below f_c as well, and relies only on the coprimality of each subarray's total number of elements (for equal-length subarrays).

Proof. To prove that between the two subarrays there is at most only one shared grating lobe position, assume the contrary. Suppose that there are two sets of co-located grating lobes at $(M\lambda/L)i = (N\lambda/L)j$ and $(M\lambda/L)i' = (N\lambda/L)j'$ (in the $\sin\theta$ domain). Thus, $M(i - i') = N(j - j')$, that is, $M/N = (j - j')/(i - i')$. However, due to Eq. (10), if $f \le f_c$, then $|j - j'| < M$ and $|i - i'| < N$, which contradicts the coprimality of M and N. □

For all frequencies below the coprime design frequency, one and only one grating lobe pair is co-located among the subarrays (the main beam). At frequencies higher than the design frequency, f_c, this no longer holds and there may be multiple sets of overlapping grating lobes, meaning there is "aliasing of the aliasing."

Because beam width depends only on wavelength and aperture length, per Eq. (4), both subarrays have the same beam width. When they are multiplied together the zeros overlap and the resulting coprime beam has angular width

$$\theta_{\text{beam}} = 2\arcsin\left(\frac{c}{Lf}\right) \tag{12}$$

for any given frequency, f. Figure 3 shows simulated coprime beampatterns' dependence on frequency.

At $f = f_c$, this reduces to

$$\theta_{\text{beam}} = 2\arcsin(2/MN) \approx 4/MN. \tag{13}$$

In other words, a coprime array with $M+N$ elements has the same main beam width as a uniform linear array with MN elements (as discussed in Sec. II A).

E. Coprime side lobe positions

The first (and most prominent) side lobes in the coprime beampattern arise from the overlap of the first two grating lobes on either side of the M- and N-array main beam. Since both subarrays are operated at the same frequency and they have the same overall length, their grating lobes are the same width [via Eq. (4)]; therefore, the maximum of their intersection happens at the average of their first lobe positions, given by Eq. (11). For a forward-facing beam (0°), these characteristic coprime side lobes occur at

$$\begin{aligned}\theta_{1(\text{Coprime})}(\lambda) &= \pm\left(\frac{\theta_{1(M)} + \theta_{1(N)}}{2}\right) \\ &= \pm\left(\frac{\arcsin\left(\frac{M\lambda}{L}\right) + \arcsin\left(\frac{N\lambda}{L}\right)}{2}\right).\end{aligned} \tag{14}$$

At $f_c = cMN/2L$ this becomes

$$\theta_{1(\text{Coprime})}(f_c) = \pm\left(\frac{\arcsin\left(\frac{2}{N}\right) + \arcsin\left(\frac{2}{M}\right)}{2}\right). \tag{15}$$

III. EXPERIMENTS AND DISCUSSION

A. Array construction

This work investigates a coprime array using 16 microphones, arranged in subarrays of 9 and 8 ("9×8"), with aperture length of 1 m. The chassis is a thin piece of acrylic with CNC-milled holes through it for microphone placement at the locations listed in Table I. The microphones used are 6.35 mm diameter omni-directional microphones (CUI Inc., Tualatin, OR) and are mounted flush with the surface of the array chassis, which provides a good seal between the calibration tool and the array. The array is 4.76 mm thick, so when the array lays flat there is minimal diffraction around the edge only above the upper limit frequency of interest. Figure 4 illustrates the 9×8 array on the large, printed protractor used for field measurement of incident angles.

TABLE I. Placement of microphones for two coprime arrays. The 9×8 array is a 1 m array with in-line subarrays of 9 and 8 elements, flush-mounted in a 4.8 mm thick acrylic chassis. The 5×4 array is a 50 cm array with in-line subarrays of 5 and 4 elements, flush-mounted in a 6.4 mm thick MDF chassis.

Element#	1	2	3	4	5	6	7	8
9×8 array mic positions (m)	0	0.11	0.125	0.22	0.25	0.33	0.375	0.44
5×4 array mic positions (m)	0	0.1	0.125	0.2	0.25	0.3	0.375	0.4
Element#	9	10	11	12	13	14	15	16
9×8 array mic positions (m)	0.5	0.55	0.625	0.67	0.75	0.78	0.875	0.89

It is advantageous to use coprime numbers that are as close together in value as possible while keeping their sum constant. The reason for this is the MN multiplication suggested in the last paragraph of Sec. II D: the beam width of a 9×8 coprime array at f_c theoretically would be $\theta_{\text{beam}} = 2\arcsin(1/72)$, whereas a 10×7 array, for instance, would be wider at $\theta_{\text{beam}} = 2\arcsin(1/70)$. The 1 m 9×8 array has $f_c = 12\,348$ Hz according to Eq. (8), which is within the frequency range of the sources and receivers available for the experiments, and consistent with the upper limit of speech spectra.

For further validating coprime theory, a second coprime array with subarrays of five and four is constructed of medium density fiberboard (MDF). It has a shorter 50 cm aperture length and uses 8 channels rather than 16, giving it an design frequency of 6860 Hz. Table I lists element placement positions for these arrays.

There could be a slight discrepancy between the two subarrays in terms of angles of incidence, because they are aligned at one side rather than at their geometric centers. However, due to the far field assumption this difference is negligible. It is assumed that the difference in incident angle between the first and last element of a given subarray is negligible; therefore, the difference between the two subarrays must also be negligible, since their geometric centers are closer together than each of their outside microphones pairs.

B. Experiment in free-field

Measurements of impulse responses between the far-field sound source and each microphone element in the coprime array are conducted in EPMAC's Studio 1 on the Rensselaer Polytechnic Institute Campus in Troy, NY, and direct sound of the measured impulse responses is windowed in the time-

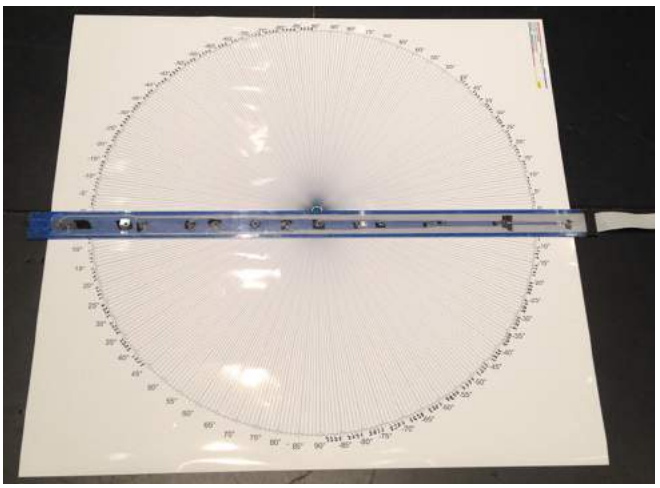

FIG. 4. (Color online) Photo of 1 m long 16-channel coprime array with subarrays of $M = 9$ and $N = 8$ positioned on a large protractor so it could be turned in precise 1° increments.

domain to exclude room reflections so as to consider the measurements being conducted in free-field. The room is 20 m long, 16 m wide, and 14 m tall. Curtains are deployed to dampen side reflections as much as possible. A sound source and the receiver (array) were placed on the rigid floor as if it were conducted in a semi-anechoic environment.

Two different experiments are conducted in the free-field condition, each using a different angle-viewing method: one uses fixed source position, and the array is turned physically using angular shifts of 1° increments, the other uses different source positions and fixed array orientation, and the array is turned virtually in discrete angles using the delay-and-sum phase shifts. The measurement procedure follows that of Ref. 18, 16-channel impulse responses measured through cross-correlation method. The output signal of the sound source is a logarithmic sweep of sine tones lasting 2 s (131 072 samples at 62.5 kHz sample frequency).

For the first experiment, the source was placed 7.33 m from the array and moved laterally by 50 cm for each successive measurement, keeping the radial distance from the array constant. The source separation distance was limited by proximity to possible reflecting surfaces in the room. For the second experiment, the source was in a fixed position 12.25 m from the array and the array was physically turned in increments of 1°. The impulse response measurement was exactly the same except only 5 averages were taken so that each measurement could be quick enough to allow time for 180 measurement angles between −90° and 90°. Alignment was slightly off: about −1° for the 9×8 coprime array and +1° for the 5×4 coprime array. Though they were visibly aligned during experimentation, asymmetry in the directional patterns can be corrected by the aforementioned angles, suggesting slight misalignment during measurement.

C. Data analysis method

The experimental impulse response data represent a relatively flat-spectrum (over the frequency range of interest) with a specific angle of incidence depending on the position of the source. These impulse responses, which are relatively free of noise, are then convolved with a signal to be located. The signal used in these experiments is a clip of pseudo-random phase noise. Due to the measurement method, the resulting data set represents an ideal case. The current experimental investigations focus is on the directional characteristic so array gain is not part of the current discussion. Adhikari and Buck[19] analytically found that detection gain for a coprime sensor array theoretically pays a penalty of about 5 dB.

1. Subarray delay-and-sum processing

Because beampatterns are frequency-dependent, the windowed signals are filtered to a narrow band of frequencies at the start of processing. The 16 channels (or 8 for the 5×4 array) of data are split into M and N channels (with the first channel being identical for each). Then within the subarrays, the delay-and-sum operation is performed with different delays corresponding to different angles of interest (angular bands). The minimum number of angular bands in 180° is MN, in order to see each lobe and zero in the pattern; however, the number of angular bands can be increased continuously, limited only by sample frequency. Time resolution can be artificially increased by up-sampling; this helps to smooth out the delay-and-sum operation, making directional responses more consistent between the first and fourth quadrants.

After delay-sum processing, the directional signals from each subarray are combined via point-by-point multiplication to get the coprime signal in that angular band. The root-mean-square (rms) value of the coprime signal is represented at the corresponding angle on the polar diagram to produce the coprime directional response. The process is repeated for as many angles as desired in order to form a complete semi-circular pattern with sufficient finite resolution.

Using boldface vector notation for time-domain data, the signals from the array elements in each subarray are processed as follows to acquire the combined coprime signal.

$$\mathbf{h}_{\text{coprime}}(\theta) = \sqrt{\sum_{m=0}^{M-1} \mathbf{h}_m e^{-j\alpha m} \times \sum_{n=0}^{N-1} \mathbf{h}_n e^{-j\alpha n}}, \tag{16}$$

where $\alpha(\theta) = 2\pi d \sin\theta / 2\lambda$. The beampattern is simply the Euclidean norm of the coprime signal, $\mathbf{h}$, as a function of angle, θ,

$$\Gamma(\theta) = |\mathbf{h}(\theta)|. \tag{17}$$

D. Fixed spatial beamforming

When the signals from all elements in a subarray are added with no delays, that subarray's beam faces forward; multiplying the two subarrays' outputs provides a forward-facing coprime beam. By changing the physical orientation of the array with respect to a fixed source (as done in the second free field experiment described in Sec. III B), the sensitivity can be recorded for each angle. These magnitudes are then normalized and presented on a polar diagram to show the coprime array's fixed beampattern. In this case angular resolution is limited by the number of impulse responses experimentally taken, but the resulting directional characteristics is an accurate representation of the true forward-facing beampattern, as shown in Fig. 5.

For fixed spatial beamforming the process can still be described by Eq. (16), but with $\theta = 0$, thus α equals zero and this becomes

$$\mathbf{h}_{\text{coprime}}(\theta) = \sqrt{\sum_{i=0}^{M-1} \mathbf{h}_i \times \sum_{j=0}^{N-1} \mathbf{h}_j}. \tag{18}$$

The Euclidean norm is then taken to achieve a single value for each angle, θ, of the beampattern.

The left column of Fig. 5 contains simulated beampatterns using Eq. (1). As previously discussed, at the design frequency the M-array ($M = 9$) contains 8 grating lobes, while the N-array ($N = 8$) contains 9 grating lobes. When the subarray signals are recorded for every angle from the experimentally measured impulse responses (shown in the right column), the grating lobes are exactly identifiable at

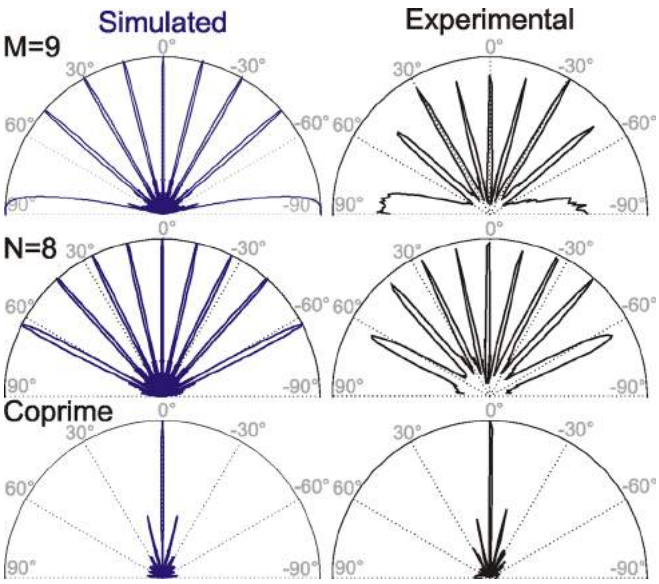

FIG. 5. (Color online) Experimental and simulated beampatterns for the 9- and 8-array subarrays, and the combined coprime array, 12th-octave filtered at $f_c = 12\,348$ Hz. Eight grating lobes of the $M = 9$ subarray and 9 grating lobes of the $N = 8$ subarray cancel one another in the coprime beam just as predicted.

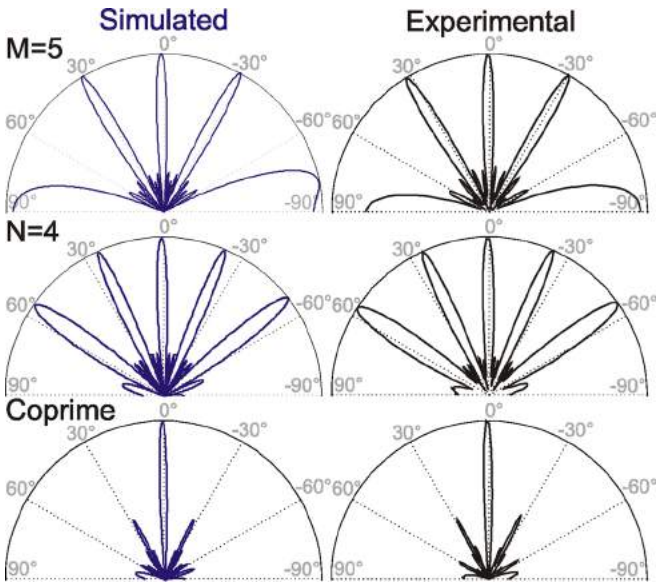

FIG. 6. (Color online) Delay-and-sum directional response of 50 cm long coprime array with subarrays of $M = 5$ and $N = 4$ for a windowed impulse response at 1° incidence. Single-frequency analysis is used at $f_c = 6.86$ kHz. Beam width and side lobe locations match predicted results. The wider beam width of this smaller array (compared to the 16-channel array) allows for greater observable detail given the 1° angular resolution of the experiment.

each predicted angle. Because the angular resolution is limited to 1°, more agreeable comparisons would require experiments with even higher spatial resolution. This is the main motivator for building a 50 cm coprime linear microphone array with subarrays of $M = 5$ and $N = 4$. Not only is the far-field condition more easily met with a shorter array, but also the design frequency is lower and the beam is not as narrow, which facilitates showing details of agreement with the simulation.

E. Delay-and-sum beamforming

By applying delay-and-sum processing, virtually turning the array in discrete shifts then recording the rms value at each angle, a directional response can be made showing the normalized pressure amplitude in each azimuthal direction. If the recorded signal only included one sound source, there should be just one peak in one angular band, and zero in all other bands. However, due to noise, reflections, diffraction, reverberation, and aliasing, there may be many smaller disturbances in the directional response. By recording in a low-noise, low-reverberation environment, cutting the signal after the direct sound, then convolving with pseudo-random noise, the only remaining influence is the aliasing pattern, which is of primary interest in this work.

The 50 cm coprime array with subarrays of $M = 5$ and $N = 4$ was tested with one normal-incident (turned out to be 1° incidence) impulse response and processed with delay-and-sum to produce directional responses at its design frequency of 6860 Hz (see Fig. 6). The resulting pattern matches the simulation almost exactly.

F. Frequency dependence

Based on the proof in Sec. II D, it is possible to use the coprime array at frequencies below f_c without misaligning the shared beam or grating lobes in a way that reduces effectiveness. Per Eq. (9), the number of grating lobes in each subarray is directly proportional to frequency. At f_c the $M = 9$ subarray has 8 grating lobes and the $N = 8$ subarray has 9 grating lobes, so at $f = 1/2f_c$ they should have 4 and 4.5 lobes, respectively. This is reflected in the experimental beampatterns in Fig. 7 when angles are adjusted by 1° to account for the slightly off-center source. Although the number of grating lobes is no longer coprime in the $f < f_c$ case,

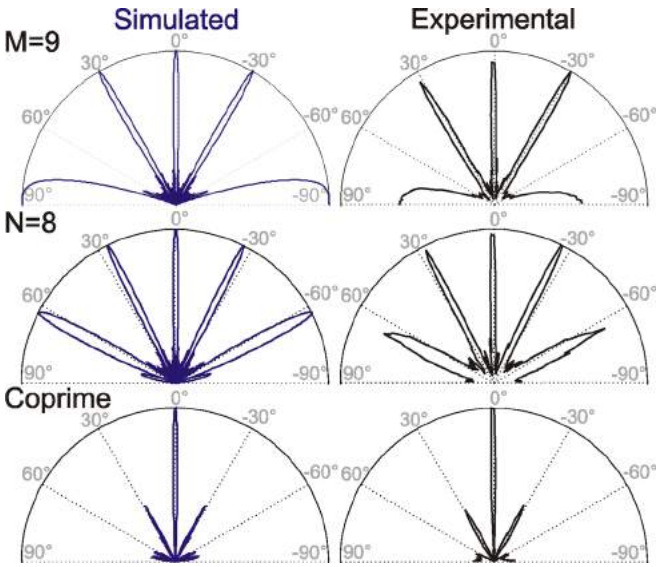

FIG. 7. (Color online) Experimental and simulated beampatterns for both subarrays and the combined coprime array, 12th-octave filtered at $f = 1/2f_c = 6.17$ kHz. This means $d_M = N\lambda/4$ and $d_N = M\lambda/4$ (instead of $\lambda/2$). Nine-array lobe positions are −90°, −30°, 0°, 31°, and 90°, and 8-array lobe positions are −64°, −25°, 0°, 27°, 64° for $f = 1/2f_c$, which agree with Eq. (11) and the simulation within ±1°.

the positioning of the lobes is still such that similar cancellation occurs. The coprimeness of the elements in the subarrays proliferates throughout the data at all frequencies lower than the design frequency. Characteristic small side lobes in the coprime beampattern are the same level as in the $f = f_c$ case (ca. -4.1 dB), but at different angles: $-28°$ and $29°$ as opposed to $-14°$ and $12°$. These agree with Eq. (14), taking into consideration ca. $1°$ misalignment.

G. Bandwidth dependence

By processing in the time domain and using a broadband source, a narrow band of frequencies is left after filtering, rather than a single frequency. The apparent effect on the normalized directional response of viewing multiple frequencies is an averaging of the normalized beampatterns corresponding to that center frequency. All directional patterns share a center beam, regardless of aliasing; however, their grating lobes occur at differing angles, therefore the side lobe magnitudes are reduced by this "averaging." This effect occurs not only in both subarray beampatterns, but in the combined coprime beampattern as well. Given a relatively flat frequency spectrum, the side lobes in the coprime beampattern are reduced with increasingly wide-frequency bandpass filters. Figure 8 shows comparisons of varying-bandwidth beampatterns against their simulations. The number of discrete frequencies needed to simulate a band of frequencies is proportional to the temporal sample frequency and the length of the data. Simulated normalized single-frequency beampatterns at these frequencies are then summed. The magnitude of each is weighted based on the magnitude of its corresponding frequency in the Fourier transform of the time-domain signal.

The 12th-octave (semitone) bandpass filtered data has a beampattern resembling that of the design frequency. As the frequency band is opened up to a third-octave ($11\,000\,\text{Hz} \leq f \leq 13\,860\,\text{Hz}$), the side lobes are drastically reduced. This effect continues as the bandwidth is opened up completely, allowing all frequencies below f_{Nyquist}.

H. Multiple-source direction of arrival estimation

By adding together two sets of 16-channel data with different source positions (impulse responses convolved with pseudo-random noise), the effect of two simultaneous sources can be emulated. First each impulse response is convolved with uncorrelated random phase white noise, then they are summed point by point. Scanning for the sound sources is then performed with the delay-and-sum method just as with the single source case.

The results of this are varied and depend heavily on side lobe activity of the juxtaposed beampatterns. As such, source locations are better identified with wider and wider bandwidth due to the side lobe mitigation. This is especially true when the sources are separated by an angle close to that of the prominent side lobes in the unweighted coprime beampattern. This happens at $13.66°$ for a coprime array with subarrays of $M = 9$ and $N = 8$ at f_c according to Eq. (15). Figure 9 shows delay-and-sum directional responses of said coprime array with center frequency $f_{\text{center}} = f_c$ viewing two simultaneous sources separated by $12°$. At this separation, the side lobes from the pattern of one source interfere constructively with those of the other, making resolution of only two sources difficult at the array's design frequency. As the bandwidth of the data is opened up, the side lobes resulting from each source diminish in the way described in Sec. III G, such that the two sources can be separated and estimation of their directions of arrival becomes possible.

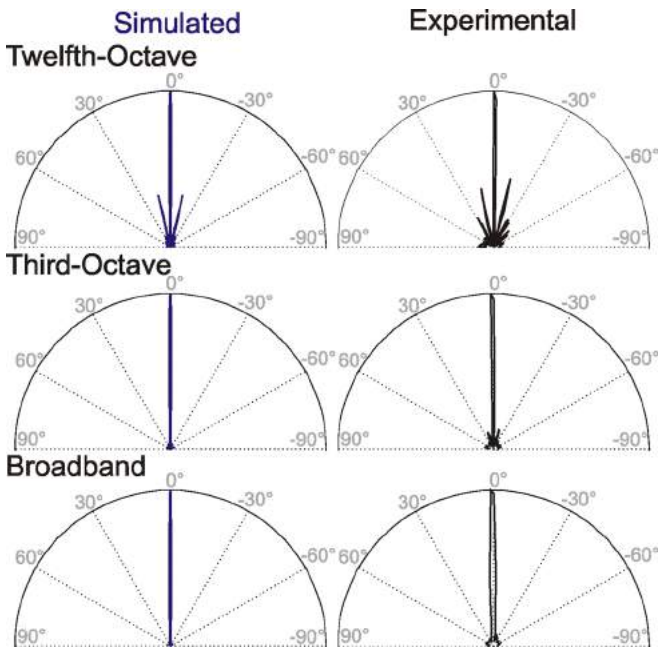

FIG. 8. (Color online) Bandpass beampatterns of a coprime array with subarrays of $M = 9$ and $N = 8$ with center frequency of $f_c = 12\,348$ Hz. Left column shows simulated beampatterns using the discrete frequencies that correspond to the frequencies present in the digital data, which depend on the sample frequency (62.5 kHz in this case). Right column shows experimental coprime beampatterns formed from the correspondingly-filtered data. The broadband data on bottom includes all frequencies up to the temporal Nyquist frequency (31.25 kHz).

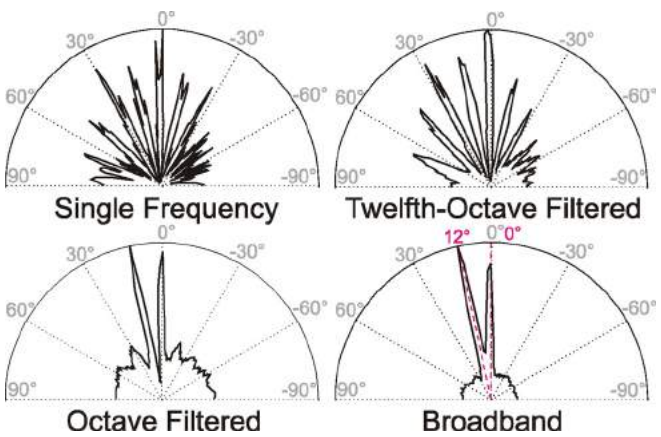

FIG. 9. (Color online) Delay-and-sum directional responses of a coprime array with subarrays of $M = 9$ and $N = 8$ with varying bandwidths centered at $f_c = 12\,348$ Hz for two uncorrelated sources at $0°$ and $12°$ incidence in a free-field condition. Because the sources are separated by the same angle as the characteristic side lobes in the unweighted coprime beampattern, their aliasing adds constructively, contributing to noise in the narrowband directional responses. As the bandwidth is increased, the side lobes die down, allowing for clear resolution of the two sources.

The Rayleigh criterion for resolution indicates that for the two sources to be resolved, the peak of one lobe must coincide with the zero of the next.[20] For lobes near 0°, their widths are close to 3.2° [per Eq. (4)], so the Rayleigh criterion should be satisfied for sources at angles $\theta_\Delta = 1.6°$ from one another. However, there must still be points sampled between the peaks to show they are separated, which implies there is also a minimum angular resolution. Assuming the peaks fall at sampled angles, there must be at least one sample between them showing a dip in magnitude—this would require angular resolution of $1.6/3 = 0.53°$. This means with experimental angular resolution of only 2.5°, the minimum resolvable angular separation between two simultaneous sources is 7.5°. Figure 10 illustrates broadband directional responses of two simultaneous sources separated by 4°, 8°, and 12°, respectively. Upsampling by 10× and increasing the number of points between −90° and 90° improves this, but not necessarily tenfold, since the added points do not accurately represent the underlying analog waveform. However, since the side lobes have a negative impact on multi-source detection, it is beneficial to look at broad frequency ranges, which increases the beam width, increasing the Rayleigh criterion angle (Fig. 10).

I. DISCUSSION

This work represents the case that array elements are in a fixed position. Pyzdek and Culver[21] examined theoretical coprime beampatterns resulting from various degrees of bowing of the linear array. Grating lobes between the two subarrays do not cancel as well in this case; however, lobe reduction can be achieved in beamforming as long as the element positions are known.

It can be advantageous for nonuniform arrays (especially planar and volumetric random arrays) to collect data using different orientations, so that these data sets create the effect of having many more array elements. For a random spherical array, one method is to physically turn the array to take further data. Since the element locations are pseudo-random, there is a distinct lack of symmetry and turning the array allows for M new points, where M is the number of array elements. Turning the array N discrete times can simulate the effect of having MN array elements. Rigelsford and Tennant[13] propose using N discrete frequencies instead of orientations to create this side lobe-reducing effect. This is akin to the proposed method of observing a band of frequencies with coprime arrays, discussed in Sec. III G.

One major advantage of this method is the ability to use data from one measurement, rather than a set of separate measurements. A possible disadvantage is that the source needs to have enough sound energy at the frequencies being sampled in order for there to be an advantage to this method. Fortunately with coprime arrays as compared to random arrays, the locations of side lobes are easily predicted with simulations and formulas presented in Sec. III E, so it may be possible to artificially reduce side lobes in post-processing.

A method for efficiently estimating direction of arrival in limited, discrete angular bands suggested by Vaidyanathan and Pal[14] and further explored by Weng and Djuri[10] makes use of the Chinese remainder theorem and may be able to take advantage of advanced uniform linear array algorithms. By shifting the subarrays with phase delays relative to one another, the main beam can be oriented to any of the MN discrete angular bands available. This allows MN bands to be monitored using only $M + N$ shifts (combined in MN ways). So for the M-array, one must only view the M angles ($2\pi/MN$ wide in the ω domain) spanned by the main lobe within any contiguous $2\pi/N$ section of the aliased domain. Once the response of this $2\pi/N$ section of the M-array and the corresponding $2\pi/M$ section of the N-array are found, each $2\pi/MN$ angular step can be mapped to the corresponding angle in the full 2π with the Chinese remainder theorem. The method of Weng and Djuri[10] uses a two-dimensional plane to map the outputs of each subarray to the corresponding complete coprime output in a continuous way. This needs to be further explored, particularly by experimental validation.

By first estimating direction of arrival in a limited range of the subarrays, it may be possible to leverage any uniform linear array direction of arrival estimation algorithm currently available for processing coprime arrays. This could include algorithms such as Root-MUSIC, ESPRIT, IQML, and Root-WSF,[22] as well as methods in compressive sensing.[8]

Though it has been shown to be possible to experimentally reproduce simulated beampatterns, the possibility of using said patterns as directional filters has yet to be further explored. Because the outputs of the subarrays are multiplied together, coprime sensing seems to lend itself to energy-based approaches such as direction of arrival estimation. Future research should investigate new processing methods which may retain signal information in order to perform spatial filtering with coprime microphone arrays.

IV. CONCLUDING REMARKS

Sparsely spaced subarrays with coprime number of elements produce grating lobes which can be mitigated by combining their outputs while retaining the main beam; this can

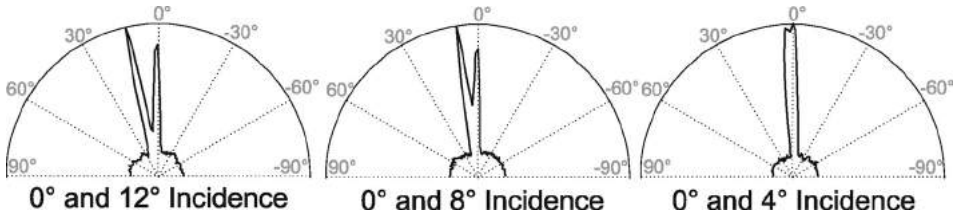

FIG. 10. Broadband directional responses of a coprime array with subarrays of $M = 9$ and $N = 8$ for simultaneous-sources in a free-field condition with varying source separations. Two sources can be clearly distinguished until they are closer in angle than the minimum resolvable angular separation of the given array with the given sampling frequency (62.5 kHz).

drastically reduce the number of elements needed to spatially resolve acoustic sources at a given frequency. Beampatterns have been simulated for various configurations of coprime arrays. Two coprime microphone arrays were constructed, one with subarrays of $M = 9$ and $N = 8$ elements for experimental validation of achievable high-frequency narrow directivity, and one with $M = 5$ and $N = 4$ elements for showing details of the beampattern. Their beampatterns were experimentally validated against the theory for the prescribed design frequency.

The coprime sparse sensing theory for direction of arrival estimation has been shown to have a directional characteristic that agrees with simulated beampatterns. Coprime theory has also been generalized to frequencies below the design frequency implied by the sparse subarray spacing, and experimental data demonstrate the coprime sparse sensing theory to be valid at the design frequency and beneath. Experimental results also show that coprime beamforming is possible and in some cases preferable with a sufficiently wide band of frequencies.

For direction of arrival estimation (of a single source or multiple sources), side lobes in the coprime pattern can be mitigated by increasing the bandwidth of the observed data. This allows for resolution of two incoherent broad-spectrum sources separated by at least 8° in the case of a coprime linear array with subarrays of $M = 9$ and $N = 8$ having a 1 m aperture.

In this work pseudo-random noise signals (convolved with the impulse response data) are used as the sources whose angle of arrival is evaluated. This could be a realistic situation for wind tunnel measurement, but future research should investigate speech or other signals that are less homogeneous temporally and spectrally. Direction of arrival estimation is sound energy based; retention of the information within the main beam's signal may be the subject of future research. This would allow for spatial filtering of speech or other signals.

Another area for further consideration is the reduction of side lobe levels in the coprime pattern. Additional array elements can narrow the grating lobes, possibly reducing the overlap which causes the highest-magnitude side lobes. This, combined with array element weightings/shading, may be able to change side lobe behavior in a favorable way.

ACKNOWLEDGMENTS

The authors are grateful to Dr. Jason Summers and Dr. Mingsian Bai for many stimulating discussions. The authors would also like to thank Jon Paul Nicols for his preliminary study in the scope of M.Sc. degree thesis at Rensselaer Polytechnic Institute.

[1]C. Bouchard, D. Havelock, and M. Bouchard, "Beamforming with microphone arrays for directional sources," J. Acoust. Soc. Am. **125**, 2098–2104 (2009).
[2]M. R. Bai, K. Hur, and Y. Liu, "Speech enhancement using an equivalent source inverse filtering-based microphone array," J. Acoust. Soc. Am. **127**, 1373–1380 (2010).
[3]J. Escolano, N. Xiang, J. M. Perez-Lorenzo, M. Cobos, and J. J. Lopez, "A Bayesian direction-of-arrival model for an undetermined number of sources using a two-microphone array," J. Acoust. Soc. Am. **135**, 742–753 (2014).
[4]K. T. Walker, M. A. Zumberge, M. A. H. Hedlin, and P. M. Shearer, "Methods for determining infrasound phase velocity direction with an array of line sensors," J. Acoust. Soc. Am. **124**, 2090–2099 (2008).
[5]G. L. D'Spain, J. C. Luby, G. R. Wilson, and R. A. Gramann, "Vector sensors and vector sensor line arrays: Comments on optimal array gain and detection," J. Acoust. Soc. Am. **120**, 171–185 (2006).
[6]D. Levin, E. A. P. Habets, and S. Gannot, "Maximum likelihood estimation of direction of arrival using an acoustic vector-sensor," J. Acoust. Soc. Am. **131**, 1240–1248 (2012).
[7]M. Crocco and A. Trucco, "The synthesis of robust broadband beamformers for equally-spaced linear arrays," J. Acoust. Soc. Am. **128**, 691–701 (2010).
[8]A. Xenaki, P. Gerstoft, and K. Mosegaard, "Compressive beamforming," J. Acoust. Soc. Am. **136**, 260–271 (2014).
[9]G. F. Edelmann and C. F. Gaumond, "Beamforming using compressive sensing," J. Acoust. Soc. Am. **130**, EL23–EL27 (2011).
[10]Z. Weng and P. M. Djuri, "A search-free DOA estimation algorithm for coprime arrays," Dig. Signal Process. **24**, 27–33 (2014).
[11]M. R. Bai, J.-G. Ih, and J. Benesty, *Acoustic Array Systems: Theory, Implementation, and Application* (John Wiley & Sons, Singapore, 2013), Chap. 6.
[12]J. Yu and K. D. Donohue, "Optimal irregular microphone distributions with enhanced beamforming performance in immersive environments," J. Acoust. Soc. Am. **134**, 2066–2077 (2013).
[13]J. M. Rigelsford and A. Tennant, "Sidelobe reduction in a random spherical volumetric array using frequency diversity," Appl. Acoust. **74** 865–869 (2013).
[14]P. P. Vaidyanathan and P. Pal, "Sparse sensing with co-prime samplers and arrays," IEEE Trans. Signal Process. **59**, 573–586 (2011).
[15]N. Xiang, D. Bush, and J. Summers, "Experimental validation of a coprime linear microphone array for high-resolution direction-of-arrival measurements," J. Acoust. Soc. Am. **137**, EL261–EL266 (2015).
[16]J. Blauert and N. Xiang, *Acoustics for Engineers* (Springer, Germany, 2008), Chap. 9.
[17]K. U. Ingard, *Fundamentals of Waves and Oscillations* (Cambridge University Press, Cambridge, UK, 1988), Chap. 1.
[18]S. Müller, "Measuring transfer-functions and impulse responses," in *Handbook of Signal Processing in Acoustics*, edited by D. Havelock, S. Kuwano, and M. Vorländer (Springer, Germany, 2008), pp. 65–85.
[19]K. Adhikari, J. Buck, and K. Wage, "Beamforming with extended coprime sensor arrays," IEEE ICASSP, 4183–4186 (2013).
[20]D. H. Johnson and D. E. Dudgeon, "Signal detection and enhancement," in *Array Signal Processing: Concepts and Techniques* (Prentice Hall, Englewood Cliffs, NJ, 1992), Chap. 1.
[21]A. Pyzdek and R. L. Culver, "Sensitivity of co-prime arrays to shape perturbation," Proc. Meet. Acoust. **19**, 070086 (2013).
[22]H. Krim and M. Viberg, "Two decades of array signal processing research," IEEE Signal Process. Mag. **13**, 67–94 (1996).